Electrochemical Detection of Free-Chlorine in Water Samples Facilitated by *in-situ* pH Control using Interdigitated Microelectrodes

Ian Seymour,[a,b] Benjamin O'Sullivan,[a] Pierre Lovera,[a] James F. Rohan,[b] and Alan O'Riordan[a]

a Nanotechnology Group, Tyndall National Institute, Cork, Ireland. E-mail: alan.oriordan@tyndall.ie

b Electrochemical Materials and Energy Group, Tyndall National Institute, Cork, Ireland. E-mail: james.rohan@tyndall.ie

KEYWORDS Chlorine sensing, Water quality monitoring, In situ pH control, Amperometric Sensor, Interdigitated array, Hypochlorous acid

ABSTRACT: Residual free-chlorine concentration in water supplies is a key metric studied to ensure disinfection. High residual chlorine concentrations lead to unpleasant odours and tastes, while low concentrations may lead to inadequate disinfection. The concentration is most commonly monitored using colorimetric techniques which require additional reagents. Electrochemical analysis offers the possibility for in-line analysis without the need for additional reagents. Electrochemical-based detection of chlorine is influenced by the solution pH, which defines the particular chlorine ionic species present in solution. As such, controlling the pH is essential to enable electrochemical based detection of residual chlorine in water. To this end, we explore the application of solid state interdigitated electrodes to tailor the in-situ pH of a solution while simultaneously detecting free-chlorine. Finite element simulations and subsequent electrochemical characterization, using gold interdigitated microelectrode arrays, were employed to explore the feasibility of an in-situ pH control approach. In practice, the approach converted residual chlorine from an initial mixture of two species (hypochlorous acid and hypochlorite ion), to one species (hypochlorous acid). Chlorine detection was shown in water samples using this exploratory method, resulting in a two-fold increase in signal response, compared to measurements without pH control. Finally, tap water samples were measured using the in-situ pH control method and the results showed excellent correlation (within experimental error) with a commercial instrument, demonstrating the efficacy of the developed technique. This work establishes the possibility of deploying an electrochemical based reagent-free, in-line chlorine sensor required for water distribution networks.

1 - Introduction

Chlorine disinfection steps are employed for both potable and non-potable water systems and, in each case, knowing the concentration of residual chlorine at the end of the distribution systems is a legal requirement. Residual chlorine is defined as the sum of the concentrations of both chlorine species, hypochlorous acid (HOCl) and hypochlorite (OCl^-).[1-3] Disinfection processes typically involve bubbling chlorine gas, or adding a salt such as sodium hypochlorite (NaOCl) to the water. Both processes result in the formation of hypochlorous acid, if the conditions are sufficiently acidic as shown by the reaction schemes:[4]

$$Cl_2 + H_2O \leftrightarrow HOCl + HCl \quad (1)$$

$$NaOCl + H_2O \leftrightarrow HOCl + NaOH \quad (2)$$

The concentration of residual chlorine in a water system must be carefully monitored since too low a value may result in ineffective disinfection and pathogens remaining in the system, while too high may lead to reactions with organic compounds forming, e.g., trihalomethanes, which have been linked to cancer,[5] respiratory problems[6] and other adverse health effects.[7] As a result, the WHO has guidelines that specify the appropriate concentrations of chlorine in drinking water.[8]

In drinking water residual chlorine typically exists as a mixture of HOCl and OCl^-, with the exact ionic ratio dependent on solution pH. Drinking water has an acceptable pH range of 6.5 to 9.5.[9] While this relatively broad pH range is suitable for human consumption, it can greatly affect the signal output from a sensor. In this pH range the chlorine ion ratio can switch from predominantly HOCl to predominantly OCl^- species; which have very different reactivities at different sensors.[10] Figure 1 shows the relationship between pH and HOCl to OCl^- ratio.[11] The standard method to detect residual chlorine is by a colorimetric technique using N,N-diethyl-p-phenylenediamine (DPD).[12] This involves the reaction between the amine group of DPD and chlorine which produces a pink coloured compound.[13] Chlorine concentration is then quantified based on the colour intensity. Similar methods have been developed based on: fluorescence, chemiluminescence and other colorimetric techniques that show high selectivity with limits of detection in the ppb range.[1-3, 14-16] Although some of these methods mitigate the issue of pH variation, they can be difficult to deploy in-line as required in water distribution networks. They also typically require the addition of a "reagent", which in most cases is not

reusable. In contrast, it is well known that electrochemical methods permit detection of other analytes without the need for additional reagents, for example, in the medtech[17, 18] and environmental sectors.[19]

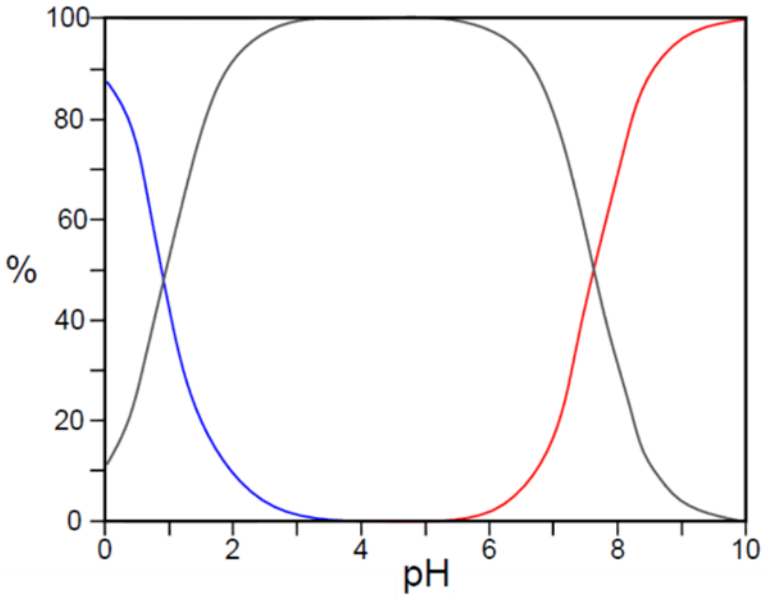

Figure 1 Distribution of residual chlorine as a function of pH, adapted from [11]. The grey line represents HOCl, the red line is OCl^- and the blue line is Cl_2.

Free-chlorine sensors have been described in the literature employing cyclic voltammetry,[20-22] linear sweep voltammetry,[23, 24] and chronoamperometry[25-30] as detection methods. Chlorine concentration is determined by measuring the reduction of either hypochlorous acid or hypochlorite according to the following reactions:[23]

$$HClO + H^+ + 2e^- \rightarrow Cl^- + H_2O \quad (3)$$

$$ClO^- + H_2O + 2e^- \rightarrow Cl^- + 2OH^- \quad (4)$$

As indicated above, the ratio of the chlorine reactants present in a measuring environment is pH sensitive. While electrochemical methods can work well in highly controlled pH environments, in unbuffered water the pH is likely to vary considerably. Equations 3 and 4 show that the reduction of the chlorine species which occur at 1.48 and 0.81 V (vs. NHE), respectively.[31, 32] The electroactivity of the chlorine species changes with pH, decreasing or increasing accordingly.[33] The reduction current associated with hypochlorous acid will decrease as the solution becomes more basic, as less hypochlorous acid is present. The same behaviour is seen with hypochlorite when the solution becomes more acidic. It is preferential to deal with hypochlorous acid in electroanalysis, as the hypochlorite reduction reaction can be influenced by the presence of dissolved oxygen.[34] As shown in figure 1, the typical pH range for drinking water can lead to different percentages of chlorine species present. Thus, it is difficult to accurately measure residual chlorine without appropriate pH control.

Prior work on the detection of mercury, has utilised *in-situ* pH control using a ring disc electrode arrangement. Hydrolysis of water produced protons at an anode ring which diffused to the sensing disc electrode lowering the pH in-situ, compared to the bulk solution and enabled direct detection.[35]. Similarly the pH can be tailored to the required value by control of the applied current density.[36] In acidic conditions, the pH can be changed through the water splitting reactions of equations 5 and 6:[37]

$$\boldsymbol{Cathode}: 2H^+ + 2e^- \rightarrow H_2 \quad (5)$$

$$\boldsymbol{Anode}: 2H_2O \rightarrow O_2 + 4H^+ + 4e^- \quad (6)$$

In basic conditions, the mechanism becomes:

$$\boldsymbol{Cathode}: 2H_2O + 2e^- \rightarrow 2OH^- + H_2 \quad (7)$$

$$\boldsymbol{Anode}: 4OH^- \rightarrow O_2 + 2H_2O + 4e^- \quad (8)$$

An acidic medium can be made more basic by consumption of protons in a reduction reaction, or alternatively more acidic by production of protons in an oxidation reaction (depending on the potential imposed at an electrode). It is important to note that the maximum pH changes occur close to the electrode and diminishes with increasing distance from the electrode.

The electrochemical measurements in this work are performed on a generator-collector type device composed of two combs of interdigitated electrode arrays. A comb here refers to one half of the interdigitated electrode array. Previous work done using similar devices has shown that interdigitated electrode arrays facilitate generator-collector electrochemistry with high efficiency.[38] The working electrodes are spaced 2 μm apart while the counter electrode is 1.1 mm away from the region of interest. By imposing an appropriate potential at one ("protonator") comb of electrodes, a pH change occurs in the local environment that tailors the pH at the other ("sensor") comb. That comb can then be used to perform sensing in conditions that differ from the bulk solution. It is vital that the counter electrode is relatively well removed spatially from the interdigitated combs. This ensures that the consumption of protons does not occur too close to the sensing electrode, which would inevitably prevent pH control. Using this approach, a local environment is created that is more acidic (or basic) than the bulk conditions. We apply this method to sensing of free-chlorine in the hypochlorous acid ionic form by electrochemically shifting the pH at a sensor to more acidic conditions. Consequently, at low pH all free-chlorine ions exist as hypochlorous acid, as shown in Figure 1, facilitating a more sensitive analysis. The close spacing of the interdigitated electrodes ensures that pH control is established by the rapid diffusion of protons, so additional convection or fluidic forces are not required. Thus, this approach has the potential for in-line analysis deployment as required, for example, in water distribution systems.

2 - Experimental Section

2.1 - Electrode Fabrication:

Silicon chip based devices were fabricated using methods similar to those described by Dawson et al.[39-41] Each chip consisted of two combs of gold working interdigitated electrodes, platinum pseudo reference and gold counter electrodes were also employed on-chip. In brief, chips were designed to interface with external electronics via a microSD port to facilitate facile electrical connection. All of the devices were fabricated on 4-inch silicon wafers bearing a thermally grown 300 nm silicon dioxide layer. Blanket metal evaporations of Titanium (10 nm) and Gold (100 nm) using a Temescal FC-2000 E-beam evaporator and lift-off technique yields interdigitated microband (55 μm x 1 μm x 60 nm) structures with gaps between the combs of 2 μm. A second metal evaporation and lift-off process yields the interconnection tracks, contact pads and the gold counter electrode (90 μm x 7 mm). Finally, a third metal evaporation was performed to create the platinum pseudo reference electrode, however an external reference electrode was used in this work. To prevent unwanted interactions along the connection tracks, silicon nitride, which acts as an insulating layer was deposited by plasma enhanced chemical vapour deposition. Photolithography and dry etching were utilised to selectively open windows (45 μm x 100 μm) in the insulating SiN layer over the microband electrodes for electrolyte access. Openings were also created over the counter and pseudo-reference electrodes and the contact pads. Each device contains six interdigitated electrode (sensors) which are separated by 0.94 mm. Once the sensor fabrication is completed, a wafer was diced into 28 separate chip devices.

A custom-made holder cell was fabricated to allow measurement in small electrolyte volumes (≈50 μL to 5 mLs.). The cell was constructed from an aluminium base and a Teflon lid. The Teflon lid was cleaned by immersion and sonication in ethanol and deionised water prior to initial use. A rinse with deionised water was performed before any electrochemical measurements. The experimental set-up is shown in supplementary figures 1 – 3. Spring loaded probes (Coda Systems Ltd. PM4J Plain Radius Microprobes) were inserted into the lid in position above the peripheral contact pads, to permit electrical connection to external potentiostats. The cell was assembled with a Viton O-ring embedded in the lid to forma seal around the on-chip electrodes. Viton O-rings were chosen for their chemical resistance. The inner diameter of the O-ring was 7 mm with a cross section of 1.6 mm to allow an opening large enough to expose all six sensors, counter and reference electrodes on the device to the electrolyte.

2.2 - Electrode Characterisation:

Each chip was inspected using optical microscopy to identify any obvious defects or faults. Prior to any electrochemical characterisation chips were cleaned by immersion in acetone, iso-propyl alcohol and finally de-ionized water, each for a period of ten minutes. The chips were dried in a flow of nitrogen and placed in the chip holder. Electrochemical analysis was performed using an Autolab Bipotentiostat (MAC80150 with BA Module, Metrohm). Cyclic voltammograms (CV) were performed from 0 V to 0.6 V at 50 mV/s in 1 mmol/L ferrocene carboxylic acid (FCA, Sigma Aldrich, 97%). During these scans, the second interdigitated comb of electrodes was held at 0 V. All electrochemical measurements were recorded versus a SCE, in solutions at room temperature (21°C).

2.3 - Buffer Preparation and Electrode Characterisation:

A series of buffers of differing pH was used to study the gold oxide reduction reaction. 0.1 mol/L citric acid (Riedel-de Haën, 99.5% anhydrous) and 0.2 mol/L sodium phosphate dibasic (Merck, 99% anhydrous) were mixed in appropriate ratios to yield buffers with pH values of 3.6, 4.6 and 7.6, respectively. 0.2 mol/L sodium phosphate dibasic and 0.2 mol/L sodium phosphate monobasic (Sigma Aldrich, 99%) were mixed to make a pH 8.6 buffer, while 0.1 mol/L sodium carbonate (Sigma Aldrich, 99%) and 0.1 mol/L sodium bicarbonate (Sigma Aldrich, 99.5%) were mixed to yield a pH 10.8 buffer. Voltammetric analysis was performed in each buffer over the potential range 0 to 1.2 V (versus SCE) at 50 mV/s.

2.4 - pH adjustment in Water Samples:

Deionised water samples and artificial drinking water (ADW) samples were used to assess the ability of the microarray to control pH. ADW was prepared by dissolving 1 g of sodium bicarbonate, 0.0654 g of magnesium sulphate (Sigma Aldrich, 99.5% anhydrous), 0.3414 g calcium sulphate dehydrate (Honeywell, 99%), 0.007 g potassium phosphate dibasic (Fluka, 98%), potassium phosphate monobasic (Sigma Aldrich, 99%) and 0.01 g sodium nitrate (Sigma Aldrich, 99%) in 10 L of deionised water. For in-situ pH control, voltammograms were performed in both DI and ADW samples by scanning the sensing comb of the IDE array from 0.2 V to 1.2 V (versus SCE) at 50 mV/s with the protonator comb biased at 1.65 V (which is in the oxygen evolution region) to protonate (acidify) the local environment of the sensing electrodes.

2.5 - Diffusion simulations:

Diffusion simulations of proton concentration in the vicinity of the protonator electrodes were undertaken according to Fick's second law. A model was designed to simulate generation at and diffusion of protons from the protonator electrodes using finite element analysis (FEA) software, COMSOL Multiphysics 5.3, in line with the galvanostatic model shown by Read et al[35]. The geometry of the model consisted of a 5 mm square box as the experimental domain, and two sets of interdigitated 1 µm wide microband electrodes (14 protonator electrodes and 13 sensing electrodes), separated by 2 µm. A flux of protons was applied at the surface of the protonators, by applying a fixed anodic current, where the flux was assumed to be proportional to the current applied at the electrodes. The initial pH value was set to 7. The proton diffusion coefficient used for the simulation was 9.31×10^{-5} cm^2 s^{-1}.[42]

2.6 - Detection of Free-Chlorine Without In-situ pH Control:

Initial scans were performed in various concentrations of free-chlorine in ADW at pH 3 (acidified using HCl) to establish the appropriate linear sweep voltammetry (LSV) parameters. Working samples were prepared by diluting Milton Sterilising Fluid (2% Sodium Hypochlorite) to the required concentrations. The concentration of free-chlorine was measured using a standard commercial free-chlorine colorimeter (Pocket Colorimeter II 58700-00 with Cl_2 Test Kit, based on the standard DPD method described earlier). The samples were acidified using 0.1 mol/L HCl to ensure the dominant chlorine ion species was hypochlorous acid. LSV potential parameters were determined to be 0.95 V to 0.2 V (versus SCE) with a 50 mV/s scan rate. Scans were also performed using the same LSV parameters at pH 8.5 to establish the detection of free-chlorine when the sample is a mixture of hypochlorous acid and hypochlorite.

2.7 - Detection of Free-Chlorine with pH Control:

The same samples of chlorine in ADW used for the tests at pH 8.5 were used for the experiments using pH control. The LSV parameters were as before with the addition of a bias of 1.65 V imposed on the protonator comb of electrodes to acidify the local environment of the sensing electrode.

3 - Results and Discussion

3.1 - Device Characterisation:

Devices were fabricated with an inter-electrode comb spacing of 2 µm. Each comb of interdigitated electrodes can be addressed separately allowing for generator-collector type sensing applications. Figure 2 (A) shows an image of a silicon chip device which consists of six sensors and on-chip counter and reference electrodes. Each sensor comprised two interdigitated electrode combs, a protonator and sensor comb, respectively. Figure 2 (B) shows a higher magnification image of a sensor with a 2 µm gap between electrode combs. The protonator comb (left hand side) contains 14 electrodes, while the sensor comb (right hand side) has 13 electrodes. The passivation is opened directly over the interdigitated combs of electrodes which is evident by the darker blue coloured rectangular window. This prevents unwanted electrochemical reactions occurring along the interconnection tracks. It is also clear that

the electrodes do not touch the opposite side of the array which indicates that there is no electrical short in the device so dual mode generator-collector type electrochemical measurements are possible.

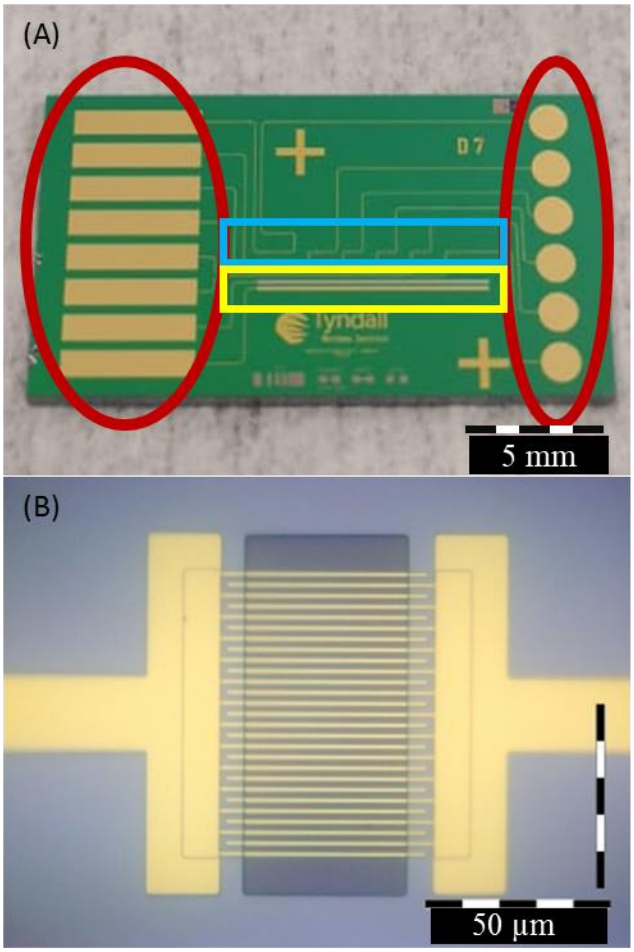

Figure 2 (A) Photograph of the full silicon chip (9.68 mm by 17.42 mm) showing contact pads (in the red circles), connection tracks, sensors (in the blue square), counter and reference electrodes (in the yellow square). (B) 50 x magnification of a single sensor array highlighting where the gold IDEs make contact to the gold pads.

Following optical inspection, the sensors were electrochemically characterized using FCA. Figure 3 shows a typical scan performed in generator-collector mode. The generator was cycled from 0 V to 0.6 V while the collector was held at 0 V. The generator comb oxidised the FCA to FCA^+. The FCA^+ species diffused across the gap to the collector electrode, which subsequently reduced it back to FCA. This is a phenomenon known as redox cycling and can be used to boost signals as described by Wahl et al.[38] The shape and current magnitude seen for the FCA scan in figure 2 was typical of a working electrode array. The voltammogram in figure 3 exhibits steady-state behavior, for the oxidation of FCA. This is a result of ultra-microelectrodes permitting time independent mass transfer when in the generator-collector mode. As such there is no overlap of diffusion layers, which would cause the array to behave as one larger electrode, diminishing sensitivity. The collection efficiency, which is a ratio of the collector to the generator currents, was determined to be 83.5 %, for 2 µm gaps. Figure 3 represents three consecutive CVs each showing excellent overlap with the previous scans demonstrating the reproducibility of the sensors. The generator voltammogram exhibited a capacitance current component arising from the fast scan rate applied. However, the collector voltammogram has a much lower capacitative current component as it was held at a constant potential throughout the experiment. Thus it's capacitance dissipated after initial biasing, evidenced by the lack of hysteresis between the forward and reverse sweeps in the collector scan of figure 3.

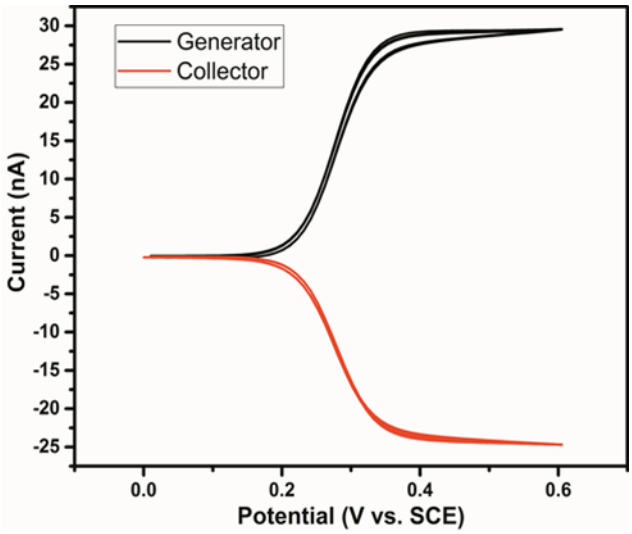

Figure 3 CVs at gold IDEs of 1 mmol/L FCA in 10 mmol/L PBS at a scan rate of 50 mV/s. The generator electrode (black) was cycled between 0 V and 0.6 V while the collector electrode (red) was held at 0 V. A current of 30 nA was indicative of a fully working array. This graph shows three consecutive cycles (N=3) each showing excellent overlap with the previous scan.

3.2 - pH Dependence of Gold Oxide Reduction Peak:

The gold oxide reduction peak was used as a probe for the pH condition of the electrodes. Gold oxide reduction is known to occur in 1 M H_2SO_4 at 1.18V vs RHE.[40] and the gold oxide reduction process is well documented (equation 9).[43]

$$Au + 3H_2O \rightleftarrows Au_2O_3 + 6H^+ + 6e^- \quad (9)$$

In alkaline solutions the oxide reduction peak potential occurs around 0.05V vs. SCE.[44] The relationship between the gold oxide peak potential thus varies approximately in a Nernstian response of 59 mV/pH unit.[45] In this work an oxide was formed on a gold electrode by scanning to a sufficiently positive potential, typically around 1.2 V. The electrode was then swept cathodically to the initial potential and the position of the oxide reduction peak was noted. This procedure was repeated at different pH values in a series of buffers to establish the linearity of the technique. Figure 4 (A) shows the oxide reduction peaks for the different buffer solutions. In each case, four replicate scans were performed to determine reproducibility. As expected, the oxide peaks shifted to more positive potentials at lower pH values. The oxide peak potential values for different pH values were reproducible (SD of 6.32 x 10^{-4}V for greatest error) over multiple scans as confirmed by the negligible error bars for the calibration in figure 4 (B) fitted using a linear regression approach. The error was calculated as three times the standard deviation between scans, which was used for each calibration. The calibration plot indicates a strong linearity with an $R^2 = 0.998$.

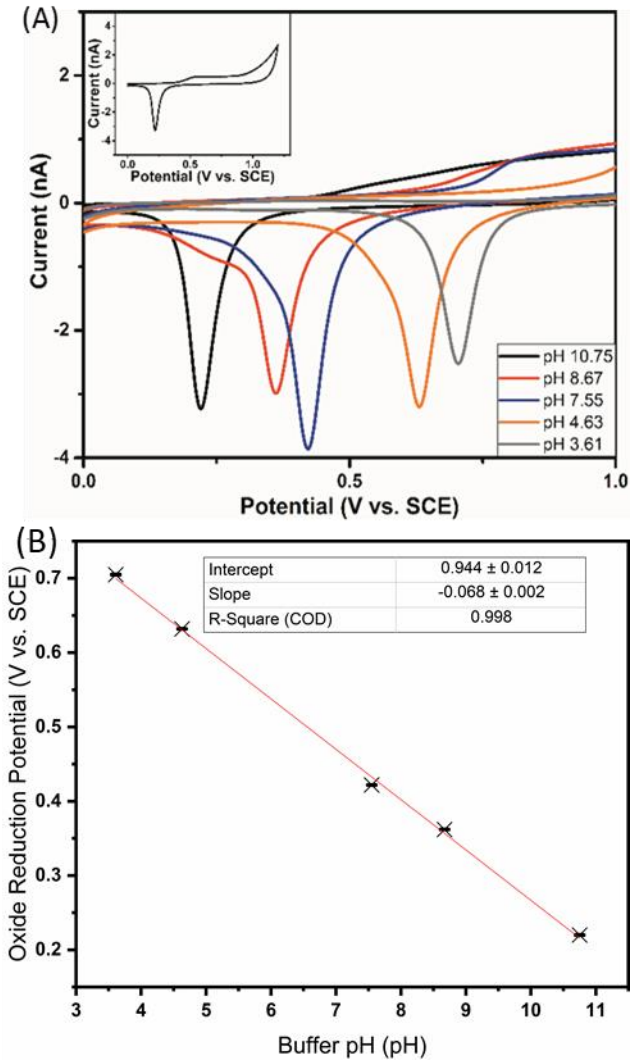

Figure 4 (A) CVs of one electrode comb in a series of pH buffers from 0 to 1.2 V at 50 mV/s. For these scans, the second electrode was left unbiased to prevent any interference (N=3). The inset shows the full scan used to take a measurement. (B) Calibration plot of oxide peak reduction potential vs. pH. A linearity fit of 0.998 is determined for this calibration plot.

The oxide reduction peak approach to pH analysis shows a sensitivity of 67.7 mV/pH, indicated by the slope of the linear fit above. The slight deviation from Nerstian behaviour may be due to the utilization of a fixed upper limit for oxide formation in the solutions of different pH.

3.3 - Simulation of pH Control at Interdigitated Electrodes:

To support the viability of the proposed in-situ pH control method using interdigitated electrodes, a simulation study was performed to assess the diffusion characteristics for H^+ ions away from a protonator electrode with 2 µm separations. The simulation model was employed to determine the best electrode configuration for pH control and to establish some of the conditions necessary to tailor the local pH values required. Figure 5 (A) shows the pH in the environment of the electrodes after applying a current of 1 µA for 10 ms. The image shows a 2-D cross-section of a 1.2 mm by 1.8 mm area through the interdigitated array. It can be seen that although the bulk pH value remains at its initial value (in this case pH 7.0), in the locality of the electrodes the pH has begun to drop from pH 7 to below pH 5 (see inset – magnified showing a 6 µm by 16 µm area around the electrodes). Figure 5 (B) shows the situation 100 ms after the current bias was applied. The diffusion layer thickness has increased and the local pH environment at the electrodes has decreased to below 4. Figure 5 (C) shows the local environment 1 s after the current bias was applied. The diffusion layer thickness has increased further and the local environment at the electrodes is now at pH 3 (Inset). This suggests that within 1 second from switching on the pH control, the local pH environment should be sufficiently low to convert all residual chlorine to hypochlorous acid ionic form.

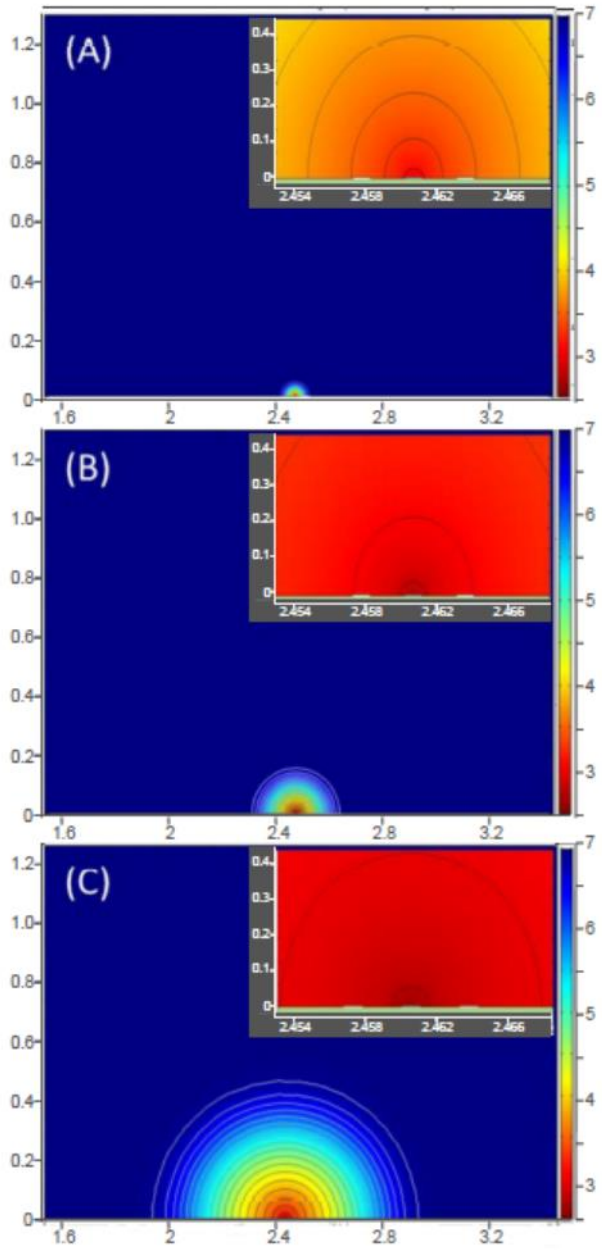

Figure 5 Simulation of an interdigitated array of electrodes with a current of 1 µA applied to the inner electrode. Simulations show the local pH 10 ms (A), 100 ms (B) and 1000 ms (C) after current imposition. The insets are a higher magnification of the 3 electrodes highlighting the local pH environment. The colour gradient represents the pH, the legend of which is shown on the right. The insets also show the silicon substrate (light green colour). The axis for each simulation is given in millimetres.

3.4 - Evaluation of in-situ pH Control of Deionised Water and Artificial Drinking Water:

The potential of the gold oxide reduction peak was used to determine the parameters required for pH control in non-buffered matrices as shown in Figure 4. Deionised water samples were used initially to minimize complications arising from buffering capacity and interfering species. The samples were made slightly basic using 10 mmol/L NaOH, to assist with the water splitting reactions at neutral pH. Tests were performed in triplicate where the sensing comb was swept anodically from 0 V to 1.2 V while the protonator remained unbiased. A gold oxide was formed on the electrode and subsequently reduced on the cathodic sweep. The location of the reduction peak maximum was observed at ~ 0.27 V, see Figure 6 (a). This indicates that the initial pH of the DI water sample was closer to pH 10. The protonator electrode was then biased at a constant positive potential of 1.65V (vs. SCE) to induce a local pH change and the sensor electrode again swept from 0 V to 1.2 V. These results are shown in figure 6(A), where the gold oxide reduction peak of the sensor electrode was observed to shift anodically to 0.75 V; a shift of 480 mV. Using the data presented in Figure 4(B) it is estimated that the induced pH change was from pH 9.8 to pH 2.9 at the “sensor” comb electrode.

Tests were then repeated in ADW to determine the effectiveness of pH control in real sample conditions. ADW contains significant concentrations of sodium bicarbonate which is an additional complication expected to buffer the pH at around 8.5. Using the same parameters as described above, it was found that pH control was still possible under these buffered conditions, see Figure 6(B). The pH shift is not as large as for deionised water, but it was still sufficient to decrease the pH. The initial oxide reduction peak was seen at 0.3 V, indicating a pH 9.3. Following the application of pH control, the oxide reduction peak appears at 0.68 V, which was estimated to be pH 3.8. While not as acidic as the deionised water sample, this pH still enables an expected total conversion to HOCl (see Figure 1). By adjusting the protonator potential further, the pH change can be tailored to the required value of 3.0.

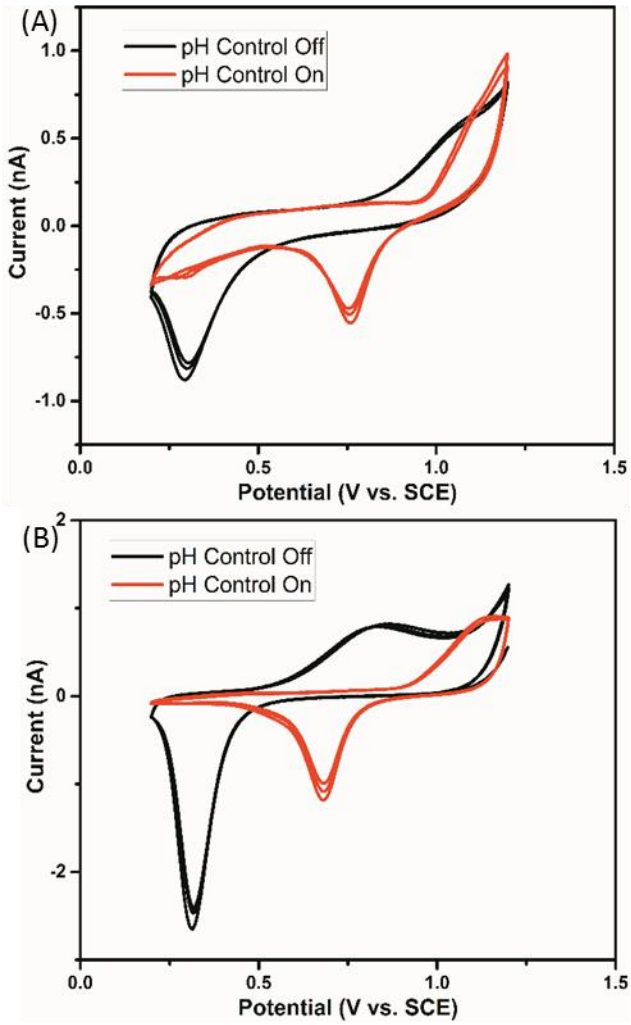

Figure 6 CVs at gold "sensor" IDE's over the range 0.2 to 1.2V vs SCE at a sweep rate of 50 mV/s. (A) Deionised water at an Initial pH is 9.8 the oxide reduction peak is seen at approximately 0.27 V (black). By biasing the second electrode at 1.65 V the oxide reduction peak shifts to 0.75 V (red)(N=3). (B) The same parameters were applied to a sample of ADW (N=3)

3.5 - Free-Chlorine Detection Using pH Control:

Samples of hypochlorous acid (made by diluting a hypochlorite stock in ADW and acidifying with 10 mM HCl) were assessed using the IDEs to establish the appropriate detection window. LSV was again used as the detection method and it was found that scanning from 0.95 V to 0.2 V at 50 mV/s was optimal for detection of free-chlorine. A series of low concentration (0.3 - 2 ppm) hypochlorous acid standards (pH of approximately 8.5) were prepared and their respective concentrations confirmed using the standard calibrated commercial DPD method. The value of pH 8.5 was chosen to ensure that the solutions were predominantly hypochlorite. Figure 7 (A) shows typical LSV scans obtained at a sensor electrode while the protonator electrode remained un-biased. Under these conditions, the free-chlorine exists as both hypochlorous acid and hypochlorite, with the latter being the predominant species. Voltammograms recorded for the 0.35 and 0.7 ppm standards overlapped entirely, as the currents associated with each are quite low, and could not be differentiated from each other. A well-defined plateau current for the reduction was not observed making it difficult to determine the appropriate potential at which to take a reading for calibration purposes. A second plateau associated with hypochlorite

reduction would be expected outside of this potential window at more cathodic potentials in the oxygen reduction region. Consequently, dissolved oxygen would interfere with the analysis by providing higher currents and thus false positive readings. The equivalent tests were then undertaken in newly prepared standard solutions acidified to pH 3 using 0.1 mol/L HCl. The equivalent LSV scans are presented in figure 7 (B). Much higher currents (compared to Figure 7(A)) for similar concentrations were observed. This higher sensitivity allowed clear discrimination between the lower concentration standards. Furthermore, a well-defined plateau region between 0.2 V to 0.3 V was observed enabling facile calibration.

Following the successful demonstration of decreasing pH increasing chlorine detection sensitivity, the protonator potential established for pH control in blank water samples was then applied to the initial free-chlorine standards at pH 8.5. Figure 7 (C) shows the equivalent scans (to figure 7 (A)) performed with the protonator biased at 1.65 V. A significant increase in signal current was observed for each scan performed; similar to Figure 7(B). A second reduction event was observed in the pH control results, occurring at approximately 0.6 V. While not fully understood, it is possible that this may arise as a result of chlorine (Cl_2) formation. As shown in figure 1, it is possible for Cl_2 to form in extremely acidic pH conditions. While the parameters used should create a pH 3.8 environment, it is possible that the pH is lower than this. This second reduction was not seen in the samples that had been chemically adjusted, as the samples could not become more acidic. Figure 7 (D) shows the associated calibration curve fitted using a linear regression technique exhibiting good linearity with a $R^2 = 0.969$ as low as 0.35 ppm. A limit of detection for this method was estimated to be 0.01 ppm, calculated using the standard error of estimate method.[46] Measurements were undertaken in triplicate on the same sensor to determine the error.

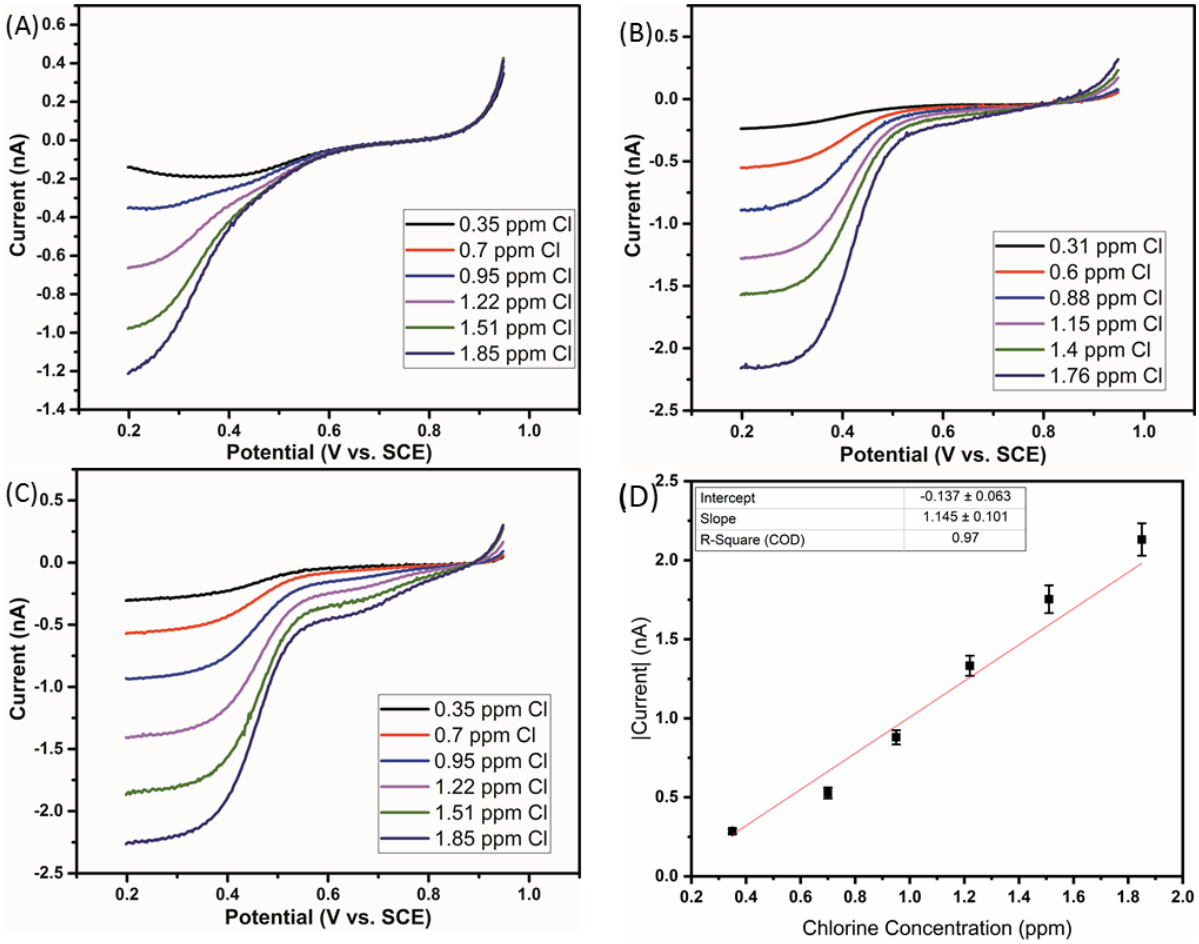

Figure 7 LSVs at gold IDE's over the range 0.95 to 0.2V vs. SCE at a sweep rate of 50 mV/s. (A) Various concentrations of chlorine measured by the DPD method in ADW at pH 8.5 (N=3). (B) Various concentrations of chlorine measured by the DPD method in ADW at pH 3 (N=3). (C) Various concentrations of chlorine measured by the DPD in ADW at pH 8.5 with the protonator electrode biased at 1.65 V (N=3). (D) Calibration plot for the scans shown in (C).

3.6 - Detection of Free-Chlorine in Tap Water Samples:

To confirm the potential of these sensors for water distribution applications, measurements of residual free-chlorine were undertaken in tap water samples. For this work, the protonator was again biased at 1.65 V. The sensing electrodes were biased at 1.2 V, to generate the gold oxide and the potential of the gold oxide reduction peak observed by scanning cathodically used to confirm pH ≈3.0 of the solution in the region of the sensing electrode. A standard addition approach was used to determine the unknown concentration of residual chlorine in tap water. An initial measurement was performed in tap water, i.e., an 'unknown' sample. Subsequent scans were

then performed in tap water samples that had been spiked with residual chlorine stock solution to form 'unknown' + 0.5, 1.5, 2.5, 3.5 and 4.5 ppm of chlorine. The resulting scans are shown in figure 8(A). A scan of the unknown sample is shown in the supplementary information (SF4). It was found that while pH 3 conditions were achieved in tap water, the HOCl reduction occurred at a less positive potential and did not reach a steady state. This was thought to be a result of some unknown component of tap water slowing the kinetics of the HOCl formation, which needs to be investigated further. However, figure 8 (B) shows that linearity was maintained and allowed for quantification of the unknown. The concentration of the base tap water sample was determined by extrapolating the linear fit to the x-axis, which has been highlighted in figure 8 (B). The value recorded by this method was 0.33 ppm. The actual concentration was determined using the commercial DPD method, which yielded a concentration of 0.31 ppm. A calibration based on the actual concentrations is shown in the supplementary information (SF5 and SF6). In this regard, both methods provided the same result within experimental error thereby confirming the efficacy of the in-situ pH control method.

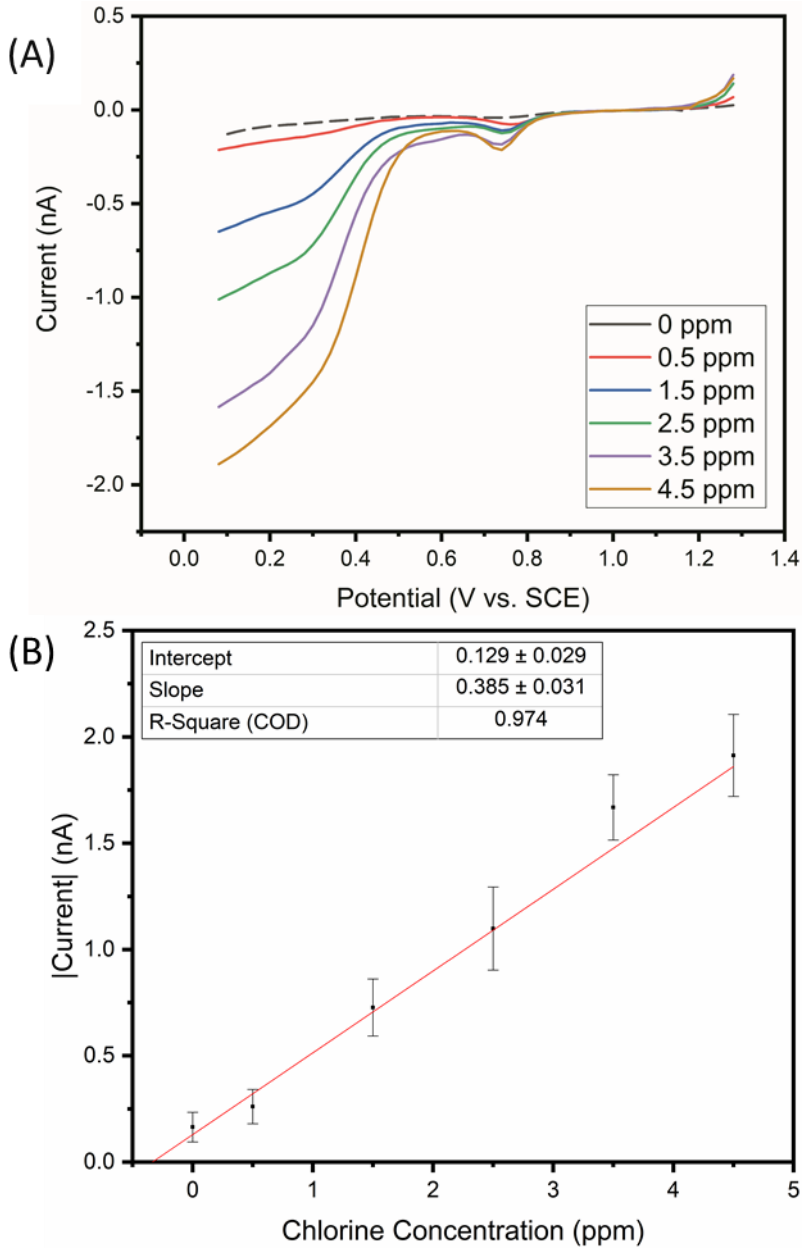

Figure 8 LSV's at gold IDE's from 1.2 V to 0 V at a sweep rate of 50 mV/s. (A) Scans of various concentrations of chlorine in tap water (N=3). The dashed line represents the unknown sample. (B) Calibration plot for the scans shown in (A)

Conclusions

We have shown that electrochemical pH control is an effective approach to detecting residual chlorine concentration in real water samples. Finite element simulations and subsequent electrochemical characterization, using gold interdigitated microelectrode arrays in buffered samples, demonstrated the feasibility of this technique. By designing the sensing electrode to be close to the protonator electrode, the local pH at the sensing electrode can be tailored to pH 3 thereby converting all free-chlorine into the hypochlorous acid species. Effective chlorine detection was shown in buffered artificial drinking water samples using in-situ pH control and an enhanced signal response, compared to measurements without pH control, was demonstrated. Finally, tap water samples were measured using the in-situ pH control method and the results correlated excellently (within experimental error) with a commercial instrument. This work shows the possibility of an electrochemical approach to reagent-free, in-line sensing of chlorine required for water distribution networks. Moreover, it highlights the potential application to other key analytes wherein detection is influenced by pH, such as heavy metals or nitrates.

AUTHOR INFORMATION

Corresponding Author

* E-mail: alan.oriordan@tyndall.ie

Author Contributions

All authors have given approval to the final version of the manuscript.

ACKNOWLEDGMENT

This publication has emanated in part from research supported by a research grant from Science Foundation Ireland and the Department of Agriculture, Food and Marine on behalf of the Government of Ireland under the Grant 16/RC/3835 (VistaMilk), and supported from research conducted with the financial support of Science Foundation Ireland (SFI) and is co-funded under the European Regional Development Fund under Grant Number 13/RC/2077 (Connect).

REFERENCES

[1] M. Szili, I. Kasik, V. Matejec, G. Nagy, B. Kovacs, Poly(luminol) based sensor array for determination of dissolved chlorine in water, Sensors and Actuators B: Chemical, 192(2014) 92-8.
[2] Y. Dong, G. Li, N. Zhou, R. Wang, Y. Chi, G. Chen, Graphene Quantum Dot as a Green and Facile Sensor for Free Chlorine in Drinking Water, Anal Chem, 84(2012) 8378-82.
[3] T. Lu, L. Zhang, M. Sun, D. Deng, Y. Su, Y. Lv, Amino-Functionalized Metal-Organic Frameworks Nanoplates-Based Energy Transfer Probe for Highly Selective Fluorescence Detection of Free Chlorine, Anal Chem, 88(2016) 3413-20.
[4] AWWA, Water Chlorination and Chloramination Practices and Principles, 2nd Edition ed.: American Water Works Association; 2011.
[5] R.D. Morris, A.-M. Audet, I.F. Angelillo, T.C. Chalmers, F. Mosteller, Chlorination, chlorination by-products, and cancer: a meta-analysis, American journal of public health, 82(1992) 955-63.
[6] B. Nemery, P. Hoet, D. Nowak, Indoor swimming pools, water chlorination and respiratory health, European Respiratory Journal, (2002).
[7] R.L. Jolley, H. Gorchev, D. Hamilton Jr, Water chlorination: environmental impact and health effects. Volume 2, Ann Arbor Science Publishers, Inc., Ann Arbor, MI1978.
[8] WHO, Monochlorine in Drinking Water, Monochlorine in Drinking Water, WHO/SDE/WSH/03.04/83 ed., World Health Organisation2004.
[9] WHO, pH in Drinking Water, pH in Drinking Water, (2007).
[10] F. Arslan, Electrooxidation as a Pretreatment Process Before Cyanidation, Nobel Metals, IntechOpen2012.
[11] M. Deborde, U. von Gunten, Reactions of chlorine with inorganic and organic compounds during water treatment—Kinetics and mechanisms: A critical review, Water Research, 42(2008) 13-51.
[12] A.P.H. Association, Standard methods for the examination of water and wastewater, APHA, 16th Ed, Washington, 309 - 15.
[13] D.L. Harp, Current Technology of Chlorine Analysis for Water and Wastewater, Technological Information Series, U.S.A., 2002.
[14] K. Singh, S.K. Mehta, Luminescent ZnO quantum dots as an efficient sensor for free chlorine detection in water, Analyst, 141(2016) 2487-92.
[15] V.V. Apyari, M.O. Gorbunova, A.V. Shevchenko, A.A. Furletov, P.A. Volkov, A.V. Garshev, et al., Towards highly selective detection using metal nanoparticles: A case of silver triangular nanoplates and chlorine, Talanta, 176(2018) 406-11.
[16] L. Lu, J. Zhang, X. Yang, Simple and selective colorimetric detection of hypochlorite based on anti-aggregation of gold nanoparticles, Sensors and Actuators B: Chemical, 184(2013) 189-95.
[17] S. Sharma, A. El-Laboudi, M. Reddy, N. Jugnee, S. Sivasubramaniyam, M. El Sharkawy, et al., A pilot study in humans of microneedle sensor arrays for continuous glucose monitoring, Analytical Methods, 10(2018) 2088-95.
[18] C. Barrett, K. Dawson, C. O'Mahony, A. O'Riordan, Development of Low Cost Rapid Fabrication of Sharp Polymer Microneedles for In Vivo Glucose Biosensing Applications, ECS Journal of Solid State Science and Technology, 4(2015) S3053-S8.
[19] I. Seymour, B. O'Sullivan, P. Lovera, J.F. Rohan, A. O'Riordan, Removal of Dissolved Oxygen Interference in the Amperometric Detection of Monochloramine Using a pH Control Method, 2019 IEEE SENSORS2019, pp. 1-4.
[20] D.R. Kumar, S. Kesavan, T.T. Nguyen, J. Hwang, C. Lamiel, J.-J. Shim, Polydopamine@electrochemically reduced graphene oxide-modified electrode for electrochemical detection of free-chlorine, Sensors and Actuators B: Chemical, 240(2017) 818-28.
[21] M. Murata, T.A. Ivandini, M. Shibata, S. Nomura, A. Fujishima, Y. Einaga, Electrochemical detection of free chlorine at highly boron-doped diamond electrodes, Journal of Electroanalytical Chemistry, 612(2008) 29-36.
[22] F. Kodera, M. Umeda, A. Yamada, Detection of Hypochlorous Acid Using Reduction Wave During Anodic Cyclic Voltammetry, Japanese Journal of Applied Physics, 44(2005) L718-L9.
[23] F. Kodera, S.-y. Kishioka, M. Umeda, A. Yamada, Electrochemical Detection of Free Chlorine Using Anodic Current, Japanese Journal of Applied Physics, 43(2004) L913-L4.
[24] M. Jović, F. Cortés-Salazar, A. Lesch, V. Amstutz, H. Bi, H.H. Girault, Electrochemical detection of free chlorine at inkjet printed silver electrodes, Journal of Electroanalytical Chemistry, 756(2015) 171-8.
[25] J. Muñoz, F. Céspedes, M. Baeza, Modified multiwalled carbon nanotube/epoxy amperometric nanocomposite sensors with CuO nanoparticles for electrocatalytic detection of free chlorine, Microchemical Journal, 122(2015) 189-96.
[26] S. Thiagarajan, Z.-Y. Wu, S.-M. Chen, Amperometric determination of sodium hypochlorite at poly MnTAPP-nano Au film modified electrode, Journal of Electroanalytical Chemistry, 661(2011) 322-8.
[27] O. Ordeig, R. Mas, J. Gonzalo, F.J. Del Campo, F.J. Muñoz, C. de Haro, Continuous Detection of Hypochlorous Acid/Hypochlorite for Water Quality Monitoring and Control, Electroanalysis, 17(2005) 1641-8.
[28] T. Soundappan, K. Haddad, S. Kavadiya, R. Raliya, P. Biswas, Crumpled graphene oxide decorated SnO_2 nanocolumns for the electrochemical detection of free chlorine, Applied Nanoscience, 7(2017) 645-53.
[29] R. Olivé-Monllau, J. Orozco, C. Fernández-Sánchez, M. Baeza, J. Bartrolí, C. Jimenez-Jorquera, et al., Flow injection analysis system based on amperometric thin-film transducers for free chlorine detection in swimming pool waters, Talanta, 77(2009) 1739-44.
[30] P. Salazar, M. Martín, J.L. González-Mora, A.R. González-Elipe, Application of Prussian Blue electrodes for amperometric detection of free chlorine in water samples using Flow Injection Analysis, Talanta, 146(2016) 410-6.
[31] O. Ordeig, R. Mas, J. Gonzalo, F. del Campo, F. Pascual, C. de Haro, Continuous Detection of Hypochlorous Acid/Hypochlorite for Water Quality Monitoring and Control, Electroanalysis, 17(2005) 1641-8.
[32] S. Fukuzaki, Mechanisms of actions of sodium hypochlorite in cleaning and disinfection processes, Biocontrol Sci, 11(2006) 147-57.
[33] F. Kodera, M. Umeda, A. Yamada, Determination of free chlorine based on anodic voltammetry using platinum, gold, and glassy carbon electrodes, Analytica Chimica Acta, 537(2005) 293-8.
[34] T. Watanabe, K. Akai, Y. Einaga, The reduction behavior of free chlorine at boron-doped diamond electrodes, Electrochemistry Communications, 70(2016) 18-22.
[35] T.L. Read, E. Bitziou, M.B. Joseph, J.V. Macpherson, In Situ Control of Local pH Using a Boron Doped Diamond Ring Disk Electrode: Optimizing Heavy Metal (Mercury) Detection, Anal Chem, 86(2014) 367-71.
[36] T.L. Read, M.B. Joseph, J.V. Macpherson, Manipulation and measurement of pH sensitive metal–ligand binding using electrochemical proton generation and metal detection, Chemical Communications, 52(2016) 1863-6.
[37] J. Rossmeisl, A. Logadottir, J.K. Nørskov, Electrolysis of water on (oxidized) metal surfaces, Chemical Physics, 319(2005) 178-84.
[38] A.J.C. Wahl, I.P. Seymour, M. Moore, P. Lovera, A. O'Riordan, J.F. Rohan, Diffusion profile simulations and enhanced iron sensing in generator-collector mode at interdigitated nanowire electrode arrays, Electrochimica Acta, 277(2018) 235-43.
[39] K. Dawson, A. Wahl, R. Murphy, A. O'Riordan, Electroanalysis at Single Gold Nanowire Electrodes, The Journal of Physical Chemistry C, 116(2012) 14665-73.

[40] K. Dawson, A. Wahl, S. Barry, C. Barrett, N. Sassiat, A.J. Quinn, et al., Fully integrated on-chip nano-electrochemical devices for electroanalytical applications, Electrochimica Acta, 115(2014) 239-46.
[41] S. Barry, K. Dawson, E. Correa, R. Goodacre, A. O'Riordan, Highly sensitive detection of nitroaromatic explosives at discrete nanowire arrays, Faraday discussions, 164(2013) 283-93.
[42] S.H. Lee, J.C. Rasaiah, Proton transfer and the mobilities of the H+ and OH– ions from studies of a dissociating model for water, The Journal of Chemical Physics, 135(2011) 124505.
[43] L. Burke, P. Nugent, The electrochemistry of gold: I the redox behaviour of the metal in aqueous media, Gold Bull, 30(1997) 43-53.
[44] L.C. Nagle, J.F. Rohan, Investigation of DMAB Oxidation at a Gold Microelectrode in Base, Electrochemical and Solid-State Letters, 8(2005) C77-C80.
[45] L.D. Burke, M.E. Lyons, D.P. Whelan, Influence of ph on the reduction of thick anodic oxide films on gold, Journal of Electroanalytical Chemistry and Interfacial Electrochemistry, 139(1982) 131-42.
[46] B. Brunetti, About Estimating the Limit of Detection by the Signal to Noise Approach, Pharmaceutica Analytica Acta, 06(2015).